

Fast Dynamic 3D Object Generation from a Single-view Video

Zijie Pan¹ Zeyu Yang¹ Xiatian Zhu² Li Zhang¹✉
¹ Fudan University ² University of Surrey

<https://fudan-zvg.github.io/Efficient4D>

Abstract

Generating dynamic three-dimensional (3D) object from a single-view video is challenging due to the lack of 4D labeled data. Existing methods extend text-to-3D pipelines by transferring off-the-shelf image generation models such as score distillation sampling, but they are slow and expensive to scale (e.g., 150 minutes per object) due to the need for back-propagating the information-limited supervision signals through a large pretrained model. To address this limitation, we propose an efficient video-to-4D object generation framework called *Efficient4D*. It generates high-quality spacetime-consistent images under different camera views, and then uses them as labeled data to directly train a novel 4D Gaussian splatting model with explicit point cloud geometry, enabling real-time rendering under continuous camera trajectories. Extensive experiments on synthetic and real videos show that *Efficient4D* offers a remarkable 10-fold increase in speed when compared to prior art alternatives while preserving the same level of innovative view synthesis quality. For example, *Efficient4D* takes only 14 minutes to model a dynamic object.

1. Introduction

Humans possess a remarkable capacity to comprehensively comprehend the spatial and temporal characteristics of a dynamic object in a brief video, even with a limited perspective, enabling them to predict its appearance in unseen viewpoints over time. Despite the significant advancement of three-dimensional (3D) object generation, existing works [4, 17, 28, 41] mostly consider static scenes or objects. With the availability of large-scale 3D datasets [5, 6], training generalizable models capable of directly generating multi-view images becomes possible [20–22]. These generated images can be turned into a 3D object through reconstruction techniques [25, 39]. By further augmenting these generated static objects with predefined animations [1], dynamic 3D content can be generated. However, this is highly

limited due to the need for fine-grained meshes as well as rigid restrictions.

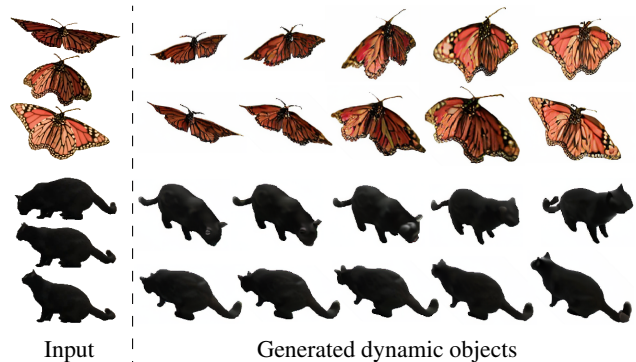


Figure 1. Examples of video-to-4D generation. **Input**: A brief video of a dynamic object, as represented by 3 frames per case; **Output**: Generated novel views at different timestamps.

Directly generating 4D object/scene content from text description has been recently attempted [36]. To bypass the need of exhaustively labeled training data pairs in form of (text, 4D), it trains a Neural Radiance Fields (NeRF)-like representation [25] via score distillation sampling [28] and separates the modeling of static scene and its dynamics. Not only is this method computationally inefficient caused by heavy supervision back-propagation through a large pretrained model, but also its textual condition is highly ambiguous in expressing the intended visual content. In quest of the aforementioned human’s capability, a recent work [10] proposed to generate dynamic 3D object images from a single-view video (statically captured monocular video from a fixed view), namely as *video-to-4D* object generation. However, similar as [36] this method is also slow to train (e.g., 150 minutes to model a single dynamic object) in addition to complex design, hence unscalable in practice.

To address identified limitations, we formulate an efficient video-to-4D object generation method in a two-staged pipeline called *Efficient4D*. In the first stage, we generate spacetime-consistent images across different camera views as synthetic training data. This is realized by imposing

✉ Corresponding to lizhangfd@fudan.edu.cn

temporal smoothing filter into a previous multi-view image generator (e.g., SyncDreamer [21]) in tandem with frame interpolation. In the second stage, we use these training data to optimize a novel 4D Gaussian splatting model. This is an extension of the recent 3D Gaussian splatting [12], originally designed for static 3D scene representation, with the temporal dimension introduced additionally on top. Using Gaussian representation brings about further computational efficiency gain along with the explicit geometry property, when compared with NeRF based designs. To tackle the discontinuity between generated frames, we design an inconsistency-aware loss function. A couple of video-to-4D results are presented in Fig. 1.

Our **contributions** are summarized as follows: (i) We consider for the first time the efficiency challenge with the under-studied video-to-4D object generation problem. (ii) We propose an efficient video-to-4D object generation pipeline, *Efficient4D*, characterized by directly generating high-quality training data without the need for heavy supervision back-propagation through a large pretrained model as suffered by most 3D/4D object generation approaches. (iii) Instead of using NeRF as the 3D representation model, we introduce a novel 4D Guardian splatting model with the real-time rendering advantage.

(iv) Extensive experiments on both synthetic and real videos validate the significant efficiency advantage (e.g., 10× speedup) of our Efficient4D over the prior art, whilst maintaining the same level of new view synthesis. Additionally, our method can also work well under the more challenging few-shot setting where only a handful of key frames are available for training, further extending the application scope.

2. Related work

4D representation Efforts to synthesize videos with free viewpoint control in dynamic scenes have a well-documented history [46]. For example, pre-NeRF [25] approaches faced challenges in reconstructing intricate scene details. Recent advancements in 4D representations, particularly those based on neural rendering, include D-NeRF [29], which decouples geometry and motion, utilizing a canonical space and a learned deformation field. HyperNeRF [27] extends the deformation field to a higher dimension, employing the level-set method for smoother optimization. DeVRF [18] reconstructs the canonical space from multi-view dense observations in the initial frame and learns the deformation field with sparse views in subsequent timesteps, utilizing a voxel grid for representation.

Similarly, deformable 3D Gaussians [44] integrates the deformation field with 3D Gaussian Splatting for the scene’s geometric structure. DyNeRF [14] extends NeRF with an additional latent code to capture detailed temporal variations, while DynIBaR [16] extends the image-

based rendering paradigm for representing long videos with complex camera and object motions. Another group of method [3, 7, 33] adopts tensor decomposition of 4D volumes to represent dynamic 3D scenes.

However, these representations often involve complex training schedules or suffer from slow convergence. In this work, drawing inspiration from 3D Gaussian Splatting [12], we propose an efficient 4D scene primitive for the representation of dynamic scenes.

3D generation 3D generation takes two main settings: text-to-3D and image-to-3D. The pioneering work, DreamFusion [28], introduces the score distillation sampling (SDS) loss for optimizing 3D shapes with diffusion models. SDS’s generality has prompted numerous subsequent efforts in both text-to-3D tasks [4, 8, 15, 17, 24, 32, 34, 38, 41, 42, 45] and image-to-3D tasks [23, 30, 37, 43] across various dimensions.

However, SDS-based approaches often suffer from extended optimization times. Conversely, some efficient methods [11, 19–21, 26] have emerged. Notably, Point-E [26] and Shap-E [11] train models to directly generate 3D point clouds or meshes. Zero123 [20] focuses on generating a 2D image from an unseen view based on a single image, convertible to a 3D shape through SDS or [19]. Importantly, SyncDreamer [21] produces multi-view consistent images, offering inspiration for reconstructing 3D objects.

4D generation There are a few recent works dedicated for more challenging 4D object generation. For instance, MAV3D [36] deals with a text-to-4D problem by training Hexplane [3] with a video diffusion model and SDS loss. Instead of text input, Consistent4D [10] conditions the generation of 4D object over time on a monocular video with richer and more specific information. However, this work is computationally inefficient due to inheriting the previous SDS loss, along with complex pipeline design. To overcome this limitation, we present a novel two-staged pipeline in a generation-and-reconstruction strategy, drastically boosting the model training speed by 10× whilst maintaining the quality of novel view synthesis.

3. Method

Our Efficient4D addresses the challenge of efficiently generating dynamic objects under novel views from a single-view video. The model, illustrated in Fig. 2, comprises two key components:

- An image synthesis pipeline (Sec. 3.1) generates images across views and timestamps, ensuring sufficient geometry and temporal consistency.
- A novel 4D Gaussian representation model (Sec. 3.2) efficiently utilizes the synthetic images for accurate dynamic

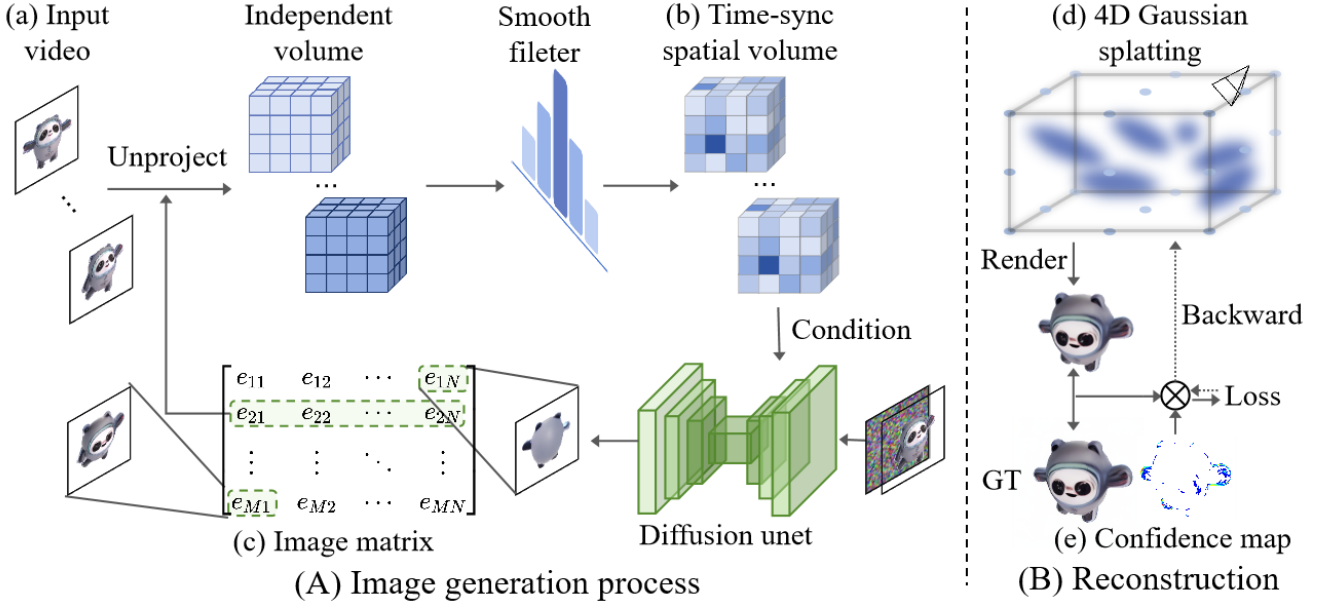


Figure 2. **Overview of our Efficient4D approach.** Given as the input a brief video depicting a dynamic object in limited perspectives, our model aims to generate this object with geometrical and temporal consistency under any specific view and time. Efficient4D comprises two components: **(A)** Image sequence synthesis across views and timestamps, resulting in (c) an *image matrix* where each row consists of multi-view geometrically consistent images and each column consists of view-specific temporally consistent images. **(B)** A novel 4D Gaussian representation model (d) that represents the scene with a number of Gaussian points. It can be trained efficiently and robustly under the confidence-aware (e) supervision on the generated image matrix.

object reconstruction and novel view synthesis.

3.1. Image synthesis across views and timestamps

Due to the difficulty of obtaining calibrated 4D scans, our approach involves the direct generation of high-quality consistent 4D data from a single-view video which is much easier to capture (Fig. 2(A)). Specifically, we seek to produce a $M \times N$ *image matrix* $\mathcal{D} = \{e_{ij}\}_{i,j=1}^{M,N}$ representing 2D images with geometrical and temporal consistency. Here, M denotes timestamps, and N represents views, with each matrix element corresponding to an image (Fig. 2(c)). This approach combines conventional video (capturing time variation, represented by a single column in the image matrix) and 3D (capturing view variation, represented by a single row in the image matrix) generation [21, 35], offering comprehensive information for modeling a dynamic object.

To initiate the image matrix \mathcal{D} , we set the first view (i.e., the first column) with K frames from the input video (Fig. 2(a)) and proceed to generate the remaining views. Our task involves generating multi-view consistent images from a single image for each row. Existing image-to-3D methods, such as SyncDreamer [21], can be leveraged for this purpose. However, these methods often struggle with temporal inconsistency within a specific view (i.e., continuity in the column direction) due to the independent synthesis

of multi-frame images. To address this issue, we propose an enhanced version of SyncDreamer with improved temporal continuity, referred to as *SyncDreamer-T*.

Specifically, SyncDreamer generates N multi-view images $\{\mathbf{x}_0^{(1)}, \dots, \mathbf{x}_0^{(N)}\}$ of a static object using a synchronized N -view noise predictor $\{\epsilon_\theta^{(n)} | n = 1, \dots, N\}$ that predicts synchronized noise for noisy multi-view images $\mathbf{x}_t^{1:N}$. The noise predictor is conditioned on information correlated with all views. Cross-view conditioning is achieved through a spatial feature volume $\mathcal{V} \in \mathbb{R}^{F \times V \times V \times V}$ unprojected by $\mathbf{x}_t^{1:N}$ to inject 3D-aware features into the shared noise predictor, ensuring geometrical consistency across views for static moments.

To impose temporal consistency, the information from \mathcal{V} at different timestamps is aggregated using a time-synchronous spatial volume we design here (Fig. 2(b)). A smoothing filter layer is introduced into the spatial volumes of different frames/timestamps, incorporating a weight vector $\mathbf{w} = (w_{-k}, \dots, w_0, \dots, w_k)$. At each denoising step, time-synchronized spatial volumes $\tilde{\mathcal{V}}_i$ for each input frame $i \in \{1, 2, \dots, M\}$ are constructed as:

$$\tilde{\mathcal{V}}_i = \sum_{j=-k}^k w_{i+j} \mathcal{V}_{i+j}. \quad (1)$$

This synchronization ensures consistent features across k

past and k future frames during the denoising process, enhancing temporal consistency.

To further improve temporal resolution, video frame interpolation (e.g., RIFE [9]) is applied after generating the image matrix \mathcal{D} as described above. The midpoint interpolation is applied twice recursively, giving three additional frames between each pair of consecutive frames. This results in a total of $M = 4K - 3$ images in a column of \mathcal{D} .

Analysis on temporal synchronization For a clearer insight into our temporal synchronization design, we undertake a simplified experiment involving two input frames, each with its feature volumes labeled as \mathcal{V}_1 and \mathcal{V}_2 . The fusion process is carried out by combining them as follows:

$$\tilde{\mathcal{V}}_i = (1 - w)\mathcal{V}_i + w\mathcal{V}_{3-i}, \quad (2)$$

where $i \in \{1, 2\}$ and w denotes the fusion ratio, we systematically vary the ratio w from 0 to 0.5, resulting in distinct columns of “Feature fusion” as illustrated in Fig. 3. For $w = 0$, the original generation process is represented, where the spatial volumes of the two frames are independent, leading to temporal inconsistency. As w approaches 0.5, we observe a gradual convergence of the generated astronauts conditioned on different input images, achieving similarity in both texture and geometry. This suggests that smoothing at the feature level is effective in aligning frames over time.

However, a challenge arises as the fused features may induce similar motion. While the bottom-left astronaut is stepping forward, the one at the bottom-right column does not exhibit forward motion like the top astronaut. Thus, a trade-off is necessary between achieving temporal consistency and preserving motion independence. In practical terms, it is recommended to set the ratio between 0.25 and 0.4, striking a balance that ensures temporal texture consistency at a moderate cost of entangled geometry.

3.2. 4D generation through reconstruction

Recall that we desire a 3D dynamic object, we should not be content with the discrete images. Our next goal is to model a truly 4D content from the image matrix \mathcal{D} . For efficient modeling, we formulate a novel 4D Gaussian representation model (Fig. 2(B)), departing from previous slow-to-train 4D reconstruction models [7].

4D Gaussian representation model Our model builds upon the 3D Gaussian splatting technique introduced in [12], originally designed for static scene representation. We extend it to address the complexities of dynamic scenes, enabling the real-time synthesis of high-fidelity views in 4D space. The model represents each Gaussian defined as:

$$G(\mathbf{p}|\mu, \Sigma) = e^{-\frac{1}{2}(\mathbf{p}-\mu)^\top \Sigma^{-1}(\mathbf{p}-\mu)}, \quad (3)$$

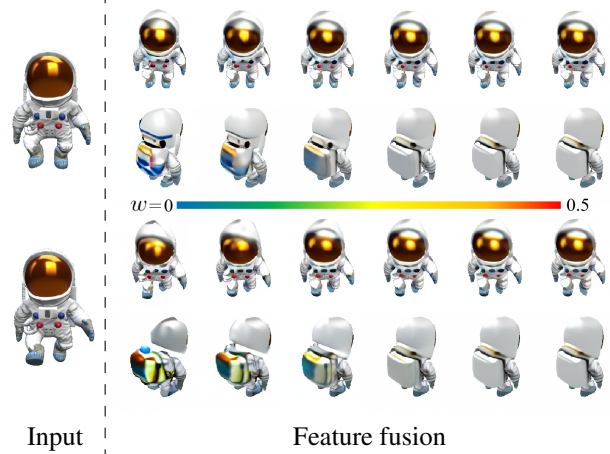


Figure 3. **Example analysis on temporal synchronization.** In this illustration, we manipulate the fusion ratio (w) across a range from 0 to 0.5 for the spatial feature volumes of two input frames. The results indicate that a moderate ratio can achieve superior outcomes by balancing both temporal consistency and motion independence.

where $\mu \in \mathbb{R}^4$ is the mean vector, and $\Sigma \in \mathbb{R}^{4 \times 4}$ is the anisotropic covariance matrix. The input $\mathbf{p} = (\mathbf{x}, t) \in \mathbb{R}^4$ represents a spacetime position with a spatial coordinate \mathbf{x} and time t . The covariance matrix Σ decomposes into a diagonal scaling matrix $S \in \mathbb{R}^{4 \times 4}$ and a rotation matrix $R \in \mathbb{R}^{4 \times 4}$ through $\Sigma = RSS^\top R^\top$. The 4D rotation R is represented by a pair of iso-rotations, each characterized by a quaternion.

In contrast to the 3D counterpart, our formulation incorporates the time dimension, allowing coherent modeling of dynamics in both space and time.

Rendering For rendering, each Gaussian includes opacity α and view-dependent color \mathbf{c} represented by spherical harmonics (SH). Given an arbitrary view \mathcal{I} defined by intrinsic and extrinsic parameters, we render the pixel at position (u, v) with timestamp t by blending visible Gaussians:

$$\mathcal{I}(u, v, t) = \sum_i f_i(u, v, t) \alpha_i \mathbf{c}_i(d) T_i \quad (4)$$

$$\text{with } T_i = \prod_{j=1}^{i-1} (1 - f_j(u, v, t) \alpha_j). \quad (5)$$

Here, i indexes the visible Gaussians sorted by depth, d refers to the direction of the pixel under the view \mathcal{I} , and $f_i(u, v, t)$ denotes the influence of a Gaussian on this position. To obtain the influence, unlike 3D Gaussian Splatting [12] which directly projects 3D Gaussians to image space, we need condition 4D Gaussians on time and then

project them. More specifically, $f(u, v, t)$ is expressed by:

$$f(u, v, t) = G_t(t|\mu_t, \Sigma_t)G_{P(\mathbf{x})|t}(u, v|P(\mu_{\mathbf{x}|t}), P(\Sigma_{\mathbf{x}|t})), \quad (6)$$

where G_t is the marginal distribution of the 4D Gaussian in time, and $G_{P(\mathbf{x})|t}$ is the projected version of the conditional 3D Gaussian with

$$\mu_{\mathbf{x}|t} = \mu_{\mathbf{x}} + \Sigma_{\mathbf{x},t}\Sigma_t^{-1}(t - \mu_t) \quad (7)$$

$$\Sigma_{\mathbf{x}|t} = \Sigma_{\mathbf{x}} - \Sigma_{\mathbf{x},t}\Sigma_t^{-1}\Sigma_{t,\mathbf{x}}. \quad (8)$$

The projection operation P [12, 47] projects the world point $\mu_{\mathbf{x}|t}$ to image space and transforms the covariance by $P(\Sigma_{\mathbf{x}|t}) = JW\Sigma_{\mathbf{x}|t}W^\top J^\top$ where W is the extrinsic matrix of \mathcal{I} and J is the Jacobian of the affine approximation of the projective transformation.

Optimization During model training, optimization is performed on the mean (μ), covariance (Σ), opacity (α), and spherical harmonic (SH) coefficients, as well as density control including densification and pruning for each Gaussian. The original objective function, as presented in [12], assumes clean training data, which may not be applicable to synthetic data with inherent imperfections. To address this, we introduce a confidence-aware objective loss formulation defined as:

$$\mathcal{L} = \lambda_{\text{rgb}}\mathcal{C}_{\text{rgb}}\mathcal{L}_{\text{rgb}} + \lambda_{\text{ssim}}\mathcal{C}_{\text{ssim}}\mathcal{L}_{\text{ssim}}, \quad (9)$$

where \mathcal{L}_{rgb} is the L_1 loss in RGB space, $\mathcal{L}_{\text{ssim}}$ is the SSIM loss [40], $\lambda_{\text{rgb/ssim}}$ is the respective weight hyper-parameter, and $\mathcal{C}_{\text{rgb/ssim}}$ is the confidence score of a generated image \mathbf{I} calculated as

$$\mathcal{C}_{\text{rgb}} = 1 - |\mathbf{I} - \hat{\mathbf{I}}|, \quad \mathcal{C}_{\text{ssim}} = \text{SSIM}(\mathbf{I}, \hat{\mathbf{I}}) \quad (10)$$

where $\hat{\mathbf{I}}$ is the unwarped image from adjacent frames estimated by the optical flow method. In such way, the confidence $\mathcal{C}_{\text{rgb/ssim}}$ function as an adaptive role in controlling the loss and gradient by assigning lower weights to inconsistent regions.

4. Experiments

4.1. Implementation details

Competitor Video-to-4D is a relatively unexplored area, with only one existing method, Consistent4D [10]. In comparison, we obtained the results of Consistent4D by referencing its original paper and project page since the source code has not been publicly released.

Evaluation videos To showcase the versatility of our proposed method, we conducted extensive experiments using a diverse set of data sources. Specifically, we focused on 20

sequences: *alpaca, astronaut, bird, butterfly, cat, corgi, dinosaur, dog, dragon, duck, flower, guard, panda, penguin, rabbit, robot, snail, Spiderman, yellow face, yoxi*.

For *dragon, guard, and yoxi*, 3D animated models were obtained from Sketchfab [2]. We rendered front-view videos and corresponding masks at 30 fps using Blender. The *yellow face* sequence was collected from the internet. To facilitate comparison with Consistent4D [10], we also conducted experiments on the videos used in their work [10].

Each sequence consists of monocular videos captured by a stationary camera, with durations ranging from approximately 1s to 6s. We uniformly selected 2-32 frames from each video as keyframes and segmented their foreground parts using SAM [13].

Implementation For time-synchronous spatial volume, we typically set the weight as $\mathbf{w} = (0.1, 0.1, 0.6, 0.1, 0.1)$. In the reconstruction stage, we implement a modified CUDA rasterizer tailored to 4D Gaussian. Gaussians are initialized randomly within the space $[-0.6, 0.6]^3$ with identity rotations and a initial number of 30,000-50,000. Training of 4D Gaussian Splatting is carried out using the Adam optimizer for 9,000 iterations with a batch size of 4. Gaussians are densified every 50 iterations, with densification halted at the 7,000th iteration. All other hyperparameters remain consistent with those in [12]. For speed efficiency, our proposed method only costs about 2 minutes for image generation and 12 minutes for reconstruction on one A6000 GPU.

4.2. Qualitative evaluation

We present qualitative comparisons in Fig. 4. In geometry rendering, we extract points at the mean of Gaussians. We also eliminate white background points and transparent points with low opacity. When assessing texture quality, it is important to note that both methods fall under the category of lifting 2D to 4D. However, Consistent4D produces watercolor-like images with low fidelity, which can be attributed to conflicts from multiple supervisory signals during prolonged optimization. In contrast, our method excels in directly generating high-quality 2D images. Subsequently, our method’s reconstruction stage yields explicit point clouds and exhibits less degradation in rendering quality compared to the SDS-based Consistent4D. Overall, our method consistently outperforms Consistent4D in most cases.

4.3. Quantitative evaluation

In Sec. 4.1, we compare Consistent4D and our method based on average generation time, rendering time, and CLIP-similarity scores [31] for input image sequences and rendered images. Measurements used the image sequences

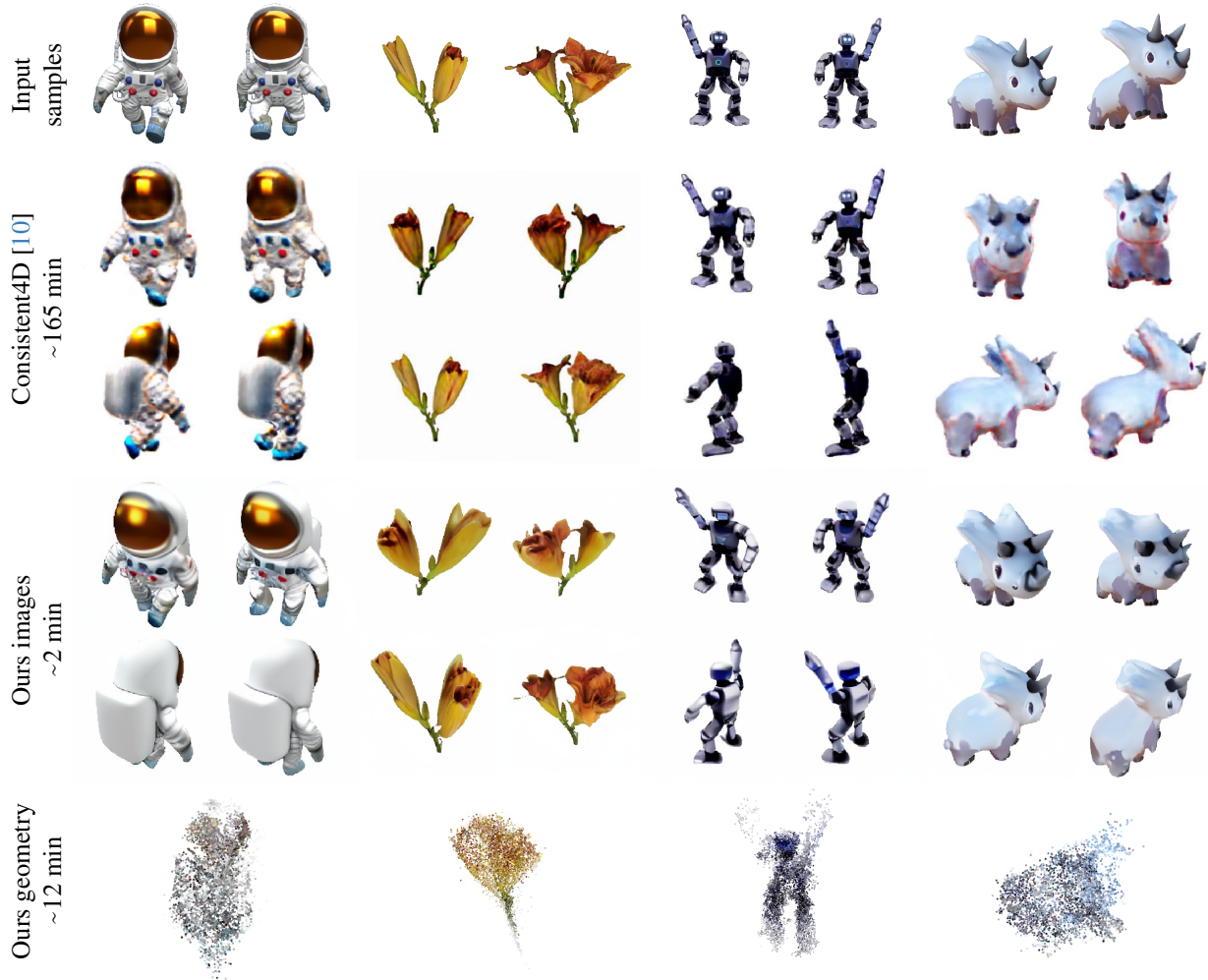


Figure 4. **Qualitative comparisons.** We show four images for each method, captured from two viewpoints at two timestamps.

Table 1. **Quantitative comparisons.** The frame per second (FPS) is evaluated using a 256×256 resolution rendering. [†]: Reported in [10] with one V100 GPU. [‡]: Measured on K-Planes [7], which partially serves as the fundamental 4D representation of Consistent4D [10].

Method	CLIP-similarity \uparrow	Generation time \downarrow	FPS \uparrow	Explicit geometry
Consistent4D [10]	0.8438	165 min [†]	~ 2 [‡]	\times
Efficient4D	0.8601	14 min	~ 1000	\checkmark

described in Sec. 4.1. Consistent4D’s CLIP-similarity evaluation is limited to RGB images from 2-3 selected views in their paper and project page, while our evaluation includes 320 images uniformly distributed in space and time, covering 16 viewpoints and 20 timestamps, making our CLIP-similarity score more robust.

We draw several observation: (1) Our method achieves superior image quality. (2) Our method significantly accelerates the generation process, achieving over $10\times$ speed improvement. (3) Our efficient 4D Gaussian representa-

tion and splatting based rendering enable real-time rendering and provide explicit point cloud geometry.

More specifically, the speed improvement is attributed to (1) our SDS-free design, converging optimization in fewer iterations, and (2) each iteration in our method requiring less time compared to Consistent4D. This time efficiency is further enhanced by avoiding recurrent evaluation in the diffusion model and prolonged forward rendering of the inefficient 4D representation as needed in the competitor at every iteration.

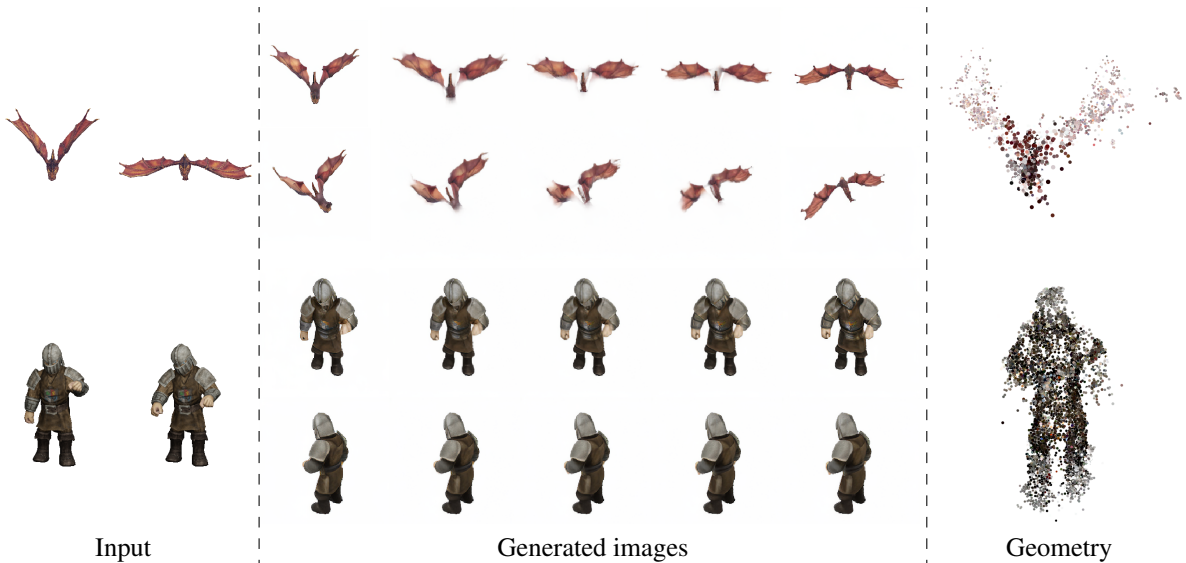


Figure 5. Given only two input frames, our method is able to generate point clouds and temporal continuous images from novel views.

4.4. Sparse input evaluation

We assessed our method’s performance in an extremely sparse input scenario, comprising only two discrete frames. In contrast, Consistent4D fails to operate effectively under such conditions. In such cases, we set $w = 0.25$ in Eq. (2). As illustrated in Fig. 5, our approach successfully generates images featuring smooth motion and high spatiotemporal consistency.

Consider a scenario where we seek 4D modeling for a static toy. While the toy can take different poses, it lacks autonomous movement, posing a challenge for continuous video capturing. In these instances, our method demonstrates effectiveness by requiring only a few key frames to produce dynamic content, thereby expanding the potential applications of the video-to-4D task.

4.5. Ablation studies

We performed ablation studies to assess the influence of different components in our approach. We compared our full method against five baseline settings: (1) Only input video are used for reconstruction; (2) Time-synchronous spatial volume is excluded; (3) Frame interpolation is excluded; (4) Confidence maps are excluded; (5) 4D Gaussian splatting is replaced with K-Plane [7]. The results corresponding to these settings can be found in Fig. 6 and Fig. 7.

Importance of synthetic data. We compare our generated image matrix with utilizing only input video using the same proposed 4D Gaussian representation model. As shown in the first row of Fig. 6, when only relying on a single-view video, the model cannot produce any meaningful results for novel views. This indicates the importance of

constructing proper training data.

Effect of time-synchronous spatial volume. We assess the impact of the time-synchronous spatial volume concept introduced in SyncDreamer, as depicted in the contrast of the second and fourth rows in Fig. 6. Without time-synchronous spatial volume, the back aspects of the toy Spiderman exhibit inconsistencies, leading to distorted geometry. In contrast, the proposed time-synchronous spatial volume enhances both spatial and temporal consistency while preventing geometry collapse, resulting in more visually appealing image generation.

Effect of frame interpolation. As illustrated in the contrast between the third and fourth rows in Fig. 6, frame interpolation is effective in mitigating the blurring observed in the rendered image from novel views. This is attributed to the low frame rates of the image matrix, which results in noticeable discontinuities.

Effect of confidence-aware in objective. The integration of a confidence-aware loss in our design serves as a strategy to mitigate training data noise. This is evident in the contrast between the third and fourth rows in Fig. 7. The inclusion of confidence maps effectively reduces blurry rendering caused by inter-frame inconsistency, resulting in a significant overall improvement in quality.

Integrating existing 4D representation model. Our synthetic training data is versatile and supports the optimization of 4D representation models, such as K-Plane [7]. In the comparison shown in Fig. 7, our 4D Gaussian splatting and K-Plane exhibit comparable proficiency in reconstructing dynamic scenes. Notably, our method surpasses K-Plane in

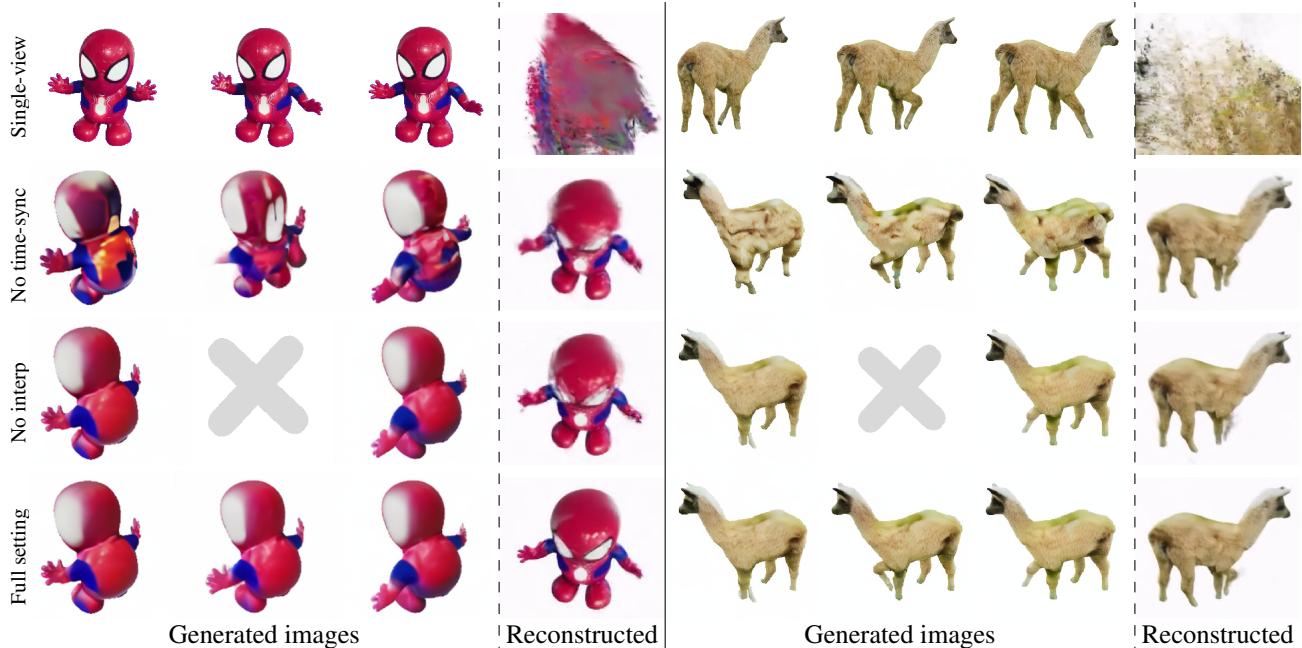


Figure 6. **Ablation study** on multi-view images generation, time-synchronous spatial volumes and frame interpolation. The images follow a chronological order from left to right.

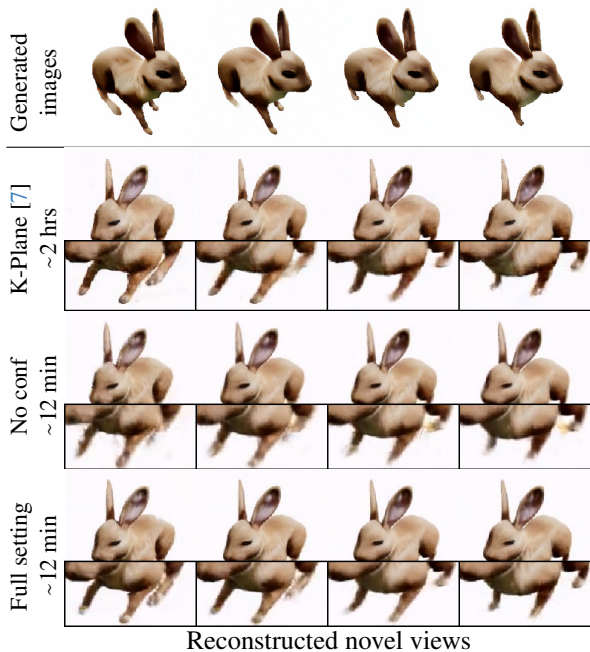


Figure 7. **Ablation study** on 4D scene representation and confidence maps. The images follow a chronological order from left to right.

speed, achieving a $10\times$ improvement. Additionally, as emphasized in Sec. 4.3, our model enables real-time rendering with explicit point cloud geometry.

5. Conclusion

This study introduces a new framework, Efficient4D, designed for generating efficiently dynamic 4D objects seamlessly from monocular videos captured by a stationary camera. The Efficient4D consists of two main stages: first, generating consistent multi-view videos with spatial and temporal coherence, and second, rapidly producing 4D object reconstructions using an innovative 4D Gaussian splatting model. Our approach, utilizing SDS-Free design and efficient 4D representation, significantly accelerates the generation process, achieving over 10 times faster speeds compared to previous work, while still delivering superior reconstruction and novel view synthesis results. Moreover, our model is effective in extremely sparse input scenarios, requiring only two available images, thereby expanding its application scope.

Limitations. Our local smoothing approach in sliding window style with our image sequence generator poses challenges in handling long-duration videos. To address this issue, replacing the smoothing filtering layer with a learnable attention layer featuring global receptive fields is a viable solution, particularly when dealing with extensive 4D datasets. Additionally, handling long videos may necessitate significant GPU memory, which can be mitigated by employing multi-GPUs or CPUs, albeit with an increase in processing time.

References

- [1] Maximo. <https://www.mixamo.com/>, 2023. 1
- [2] Sketchfab. <https://sketchfab.com/>, 2023. 5
- [3] Ang Cao and Justin Johnson. Hexplane: A fast representation for dynamic scenes. In *ICCV*, 2023. 2
- [4] Rui Chen, Yongwei Chen, Ningxin Jiao, and Kui Jia. Fantasia3d: Disentangling geometry and appearance for high-quality text-to-3d content creation. In *ICCV*, 2023. 1, 2
- [5] Matt Deitke, Ruoshi Liu, Matthew Wallingford, Huong Ngo, Oscar Michel, Aditya Kusupati, Alan Fan, Christian Laforte, Vikram Voleti, Samir Yitzhak Gadre, et al. Objaverse-xl: A universe of 10m+ 3d objects. *arXiv preprint*, 2023. 1
- [6] Matt Deitke, Dustin Schwenk, Jordi Salvador, Luca Weihs, Oscar Michel, Eli VanderBilt, Ludwig Schmidt, Kiana Ehsani, Aniruddha Kembhavi, and Ali Farhadi. Objaverse: A universe of annotated 3d objects. In *CVPR*, 2023. 1
- [7] Sara Fridovich-Keil, Giacomo Meanti, Frederik Rahbæk Warburg, Benjamin Recht, and Angjoo Kanazawa. K-planes: Explicit radiance fields in space, time, and appearance. In *CVPR*, 2023. 2, 4, 6, 7, 8
- [8] Yukun Huang, Jianan Wang, Yukai Shi, Xianbiao Qi, Zheng-Jun Zha, and Lei Zhang. Dreamtime: An improved optimization strategy for text-to-3d content creation. *arXiv preprint*, 2023. 2
- [9] Zhewei Huang, Tianyuan Zhang, Wen Heng, Boxin Shi, and Shuchang Zhou. Real-time intermediate flow estimation for video frame interpolation. In *ECCV*, 2022. 4
- [10] Yanqin Jiang, Li Zhang, Jin Gao, Weimin Hu, and Yao Yao. Consistent4d: Consistent 360° dynamic object generation from monocular video. *arxiv*, 2023. 1, 2, 5, 6
- [11] Heewoo Jun and Alex Nichol. Shap-e: Generating conditional 3d implicit functions. *arXiv preprint*, 2023. 2
- [12] Bernhard Kerbl, Georgios Kopanas, Thomas Leimkühler, and George Drettakis. 3d gaussian splatting for real-time radiance field rendering. In *ACM TOG*, 2023. 2, 4, 5
- [13] Alexander Kirillov, Eric Mintun, Nikhila Ravi, Hanzi Mao, Chloe Rolland, Laura Gustafson, Tete Xiao, Spencer Whitehead, Alexander C. Berg, Wan-Yen Lo, Piotr Dollár, and Ross Girshick. Segment anything. In *ICCV*, 2023. 5
- [14] Tianye Li, Mira Slavcheva, Michael Zollhoefer, Simon Green, Christoph Lassner, Changil Kim, Tanner Schmidt, Steven Lovegrove, Michael Goesele, Richard Newcombe, et al. Neural 3d video synthesis from multi-view video. In *CVPR*, 2022. 2
- [15] Yuhan Li, Yishun Dou, Yue Shi, Yu Lei, Xuanhong Chen, Yi Zhang, Peng Zhou, and Bingbing Ni. Focaldreamer: Text-driven 3d editing via focal-fusion assembly. *arXiv preprint*, 2023. 2
- [16] Zhengqi Li, Qianqian Wang, Forrester Cole, Richard Tucker, and Noah Snavely. Dynibar: Neural dynamic image-based rendering. In *CVPR*, 2023. 2
- [17] Chen-Hsuan Lin, Jun Gao, Luming Tang, Towaki Takikawa, Xiaohui Zeng, Xun Huang, Karsten Kreis, Sanja Fidler, Ming-Yu Liu, and Tsung-Yi Lin. Magic3d: High-resolution text-to-3d content creation. In *CVPR*, 2023. 1, 2
- [18] Jia-Wei Liu, Yan-Pei Cao, Weijia Mao, Wenqiao Zhang, David Junhao Zhang, Jussi Keppo, Ying Shan, Xiaohu Qie, and Mike Zheng Shou. Devrf: Fast deformable voxel radiance fields for dynamic scenes. *NeurIPS*, 2022. 2
- [19] Minghua Liu, Chao Xu, Haian Jin, Linghao Chen, Zexiang Xu, Hao Su, et al. One-2-3-45: Any single image to 3d mesh in 45 seconds without per-shape optimization. *arXiv preprint*, 2023. 2
- [20] Ruoshi Liu, Rundi Wu, Basile Van Hoorick, Pavel Tokmakov, Sergey Zakharov, and Carl Vondrick. Zero-1-to-3: Zero-shot one image to 3d object. In *ICCV*, 2023. 1, 2
- [21] Yuan Liu, Cheng Lin, Zijiao Zeng, Xiaoxiao Long, Lingjie Liu, Taku Komura, and Wenping Wang. Syncdreamer: Learning to generate multiview-consistent images from a single-view image. *arXiv preprint*, 2023. 2, 3
- [22] Xiaoxiao Long, Yuan-Chen Guo, Cheng Lin, Yuan Liu, Zhiyang Dou, Lingjie Liu, Yuexin Ma, Song-Hai Zhang, Marc Habermann, Christian Theobalt, et al. Wonder3d: Single image to 3d using cross-domain diffusion. *arXiv preprint*, 2023. 1
- [23] Luke Melas-Kyriazi, Iro Laina, Christian Rupprecht, and Andrea Vedaldi. Realfusion: 360deg reconstruction of any object from a single image. In *CVPR*, 2023. 2
- [24] Gal Metzger, Elad Richardson, Or Patashnik, Raja Giryes, and Daniel Cohen-Or. Latent-nerf for shape-guided generation of 3d shapes and textures. In *CVPR*, 2023. 2
- [25] Ben Mildenhall, Pratul P Srinivasan, Matthew Tancik, Jonathan T Barron, Ravi Ramamoorthi, and Ren Ng. Nerf: Representing scenes as neural radiance fields for view synthesis. *Communications of the ACM*, 2021. 1, 2
- [26] Alex Nichol, Heewoo Jun, Prafulla Dhariwal, Pamela Mishkin, and Mark Chen. Point-e: A system for generating 3d point clouds from complex prompts. *arXiv preprint*, 2022. 2
- [27] Keunhong Park, Utkarsh Sinha, Peter Hedman, Jonathan T Barron, Sofien Bouaziz, Dan B Goldman, Ricardo Martin-Brualla, and Steven M Seitz. Hypernerf: a higher-dimensional representation for topologically varying neural radiance fields. In *ACM TOG*, 2021. 2
- [28] Ben Poole, Ajay Jain, Jonathan T. Barron, and Ben Mildenhall. Dreamfusion: Text-to-3d using 2d diffusion. In *ICLR*, 2023. 1, 2
- [29] Albert Pumarola, Enric Corona, Gerard Pons-Moll, and Francesc Moreno-Noguer. D-nerf: Neural radiance fields for dynamic scenes. In *CVPR*, 2021. 2
- [30] Guocheng Qian, Jinjie Mai, Abdullah Hamdi, Jian Ren, Aliaksandr Siarohin, Bing Li, Hsin-Ying Lee, Ivan Skokhodov, Peter Wonka, Sergey Tulyakov, et al. Magic123: One image to high-quality 3d object generation using both 2d and 3d diffusion priors. *arXiv preprint*, 2023. 2
- [31] Alec Radford, Jong Wook Kim, Chris Hallacy, Aditya Ramesh, Gabriel Goh, Sandhini Agarwal, Girish Sastry, Amanda Askell, Pamela Mishkin, Jack Clark, et al. Learning transferable visual models from natural language supervision. In *ICML*, 2021. 5
- [32] Junyoung Seo, Wooseok Jang, Min-Seop Kwak, Jaehoon Ko, Hyeonsu Kim, Junho Kim, Jin-Hwa Kim, Jiyoung Lee, and Seungryong Kim. Let 2d diffusion model know 3d-consistency for robust text-to-3d generation. *arXiv preprint*, 2023. 2

- [33] Ruizhi Shao, Zerong Zheng, Hanzhang Tu, Boning Liu, Hongwen Zhang, and Yebin Liu. Tensor4d: Efficient neural 4d decomposition for high-fidelity dynamic reconstruction and rendering. In *CVPR*, 2023. 2
- [34] Yichun Shi, Peng Wang, Jianglong Ye, Mai Long, Kejie Li, and Xiao Yang. Mvdream: Multi-view diffusion for 3d generation. *arXiv preprint*, 2023. 2
- [35] Uriel Singer, Adam Polyak, Thomas Hayes, Xi Yin, Jie An, Songyang Zhang, Qiyuan Hu, Harry Yang, Oron Ashual, Oran Gafni, et al. Make-a-video: Text-to-video generation without text-video data. *arXiv preprint*, 2022. 3
- [36] Uriel Singer, Shelly Sheynin, Adam Polyak, Oron Ashual, Iurii Makarov, Filippos Kokkinos, Naman Goyal, Andrea Vedaldi, Devi Parikh, Justin Johnson, et al. Text-to-4d dynamic scene generation. In *ICML*, 2023. 1, 2
- [37] Junshu Tang, Tengfei Wang, Bo Zhang, Ting Zhang, Ran Yi, Lizhuang Ma, and Dong Chen. Make-it-3d: High-fidelity 3d creation from a single image with diffusion prior. *arXiv preprint*, 2023. 2
- [38] Christina Tsalicoglou, Fabian Manhardt, Alessio Tonioni, Michael Niemeyer, and Federico Tombari. Textmesh: Generation of realistic 3d meshes from text prompts. In *3D vision*, 2024. 2
- [39] Peng Wang, Lingjie Liu, Yuan Liu, Christian Theobalt, Taku Komura, and Wenping Wang. Neus: Learning neural implicit surfaces by volume rendering for multi-view reconstruction. In *NeurIPS*, 2021. 1
- [40] Zhou Wang, Alan C Bovik, Hamid R Sheikh, and Eero P Simoncelli. Image quality assessment: from error visibility to structural similarity. *IEEE TIP*, 2004. 5
- [41] Zhengyi Wang, Cheng Lu, Yikai Wang, Fan Bao, Chongxuan Li, Hang Su, and Jun Zhu. Prolificdreamer: High-fidelity and diverse text-to-3d generation with variational score distillation. In *NeurIPS*, 2023. 1, 2
- [42] Jinbo Wu, Xiaobo Gao, Xing Liu, Zhengyang Shen, Chen Zhao, Haocheng Feng, Jingtuo Liu, and Errui Ding. Hd-fusion: Detailed text-to-3d generation leveraging multiple noise estimation. *arXiv preprint*, 2023. 2
- [43] DeJia Xu, Yifan Jiang, Peihao Wang, Zhiwen Fan, Yi Wang, and Zhangyang Wang. Neurallift-360: Lifting an in-the-wild 2d photo to a 3d object with 360deg views. In *CVPR*, 2023. 2
- [44] Ziyi Yang, Xinyu Gao, Wen Zhou, Shaohui Jiao, Yuqing Zhang, and Xiaogang Jin. Deformable 3d gaussians for high-fidelity monocular dynamic scene reconstruction. *arXiv preprint*, 2023. 2
- [45] Joseph Zhu and Peiye Zhuang. Hifa: High-fidelity text-to-3d with advanced diffusion guidance. *arXiv preprint*, 2023. 2
- [46] C Lawrence Zitnick, Sing Bing Kang, Matthew Uyttendaele, Simon Winder, and Richard Szeliski. High-quality video view interpolation using a layered representation. *ACM TOG*, 2004. 2
- [47] Zwicker, Pfister, Van Baar, and Gross. Ewa volume splatting. In *Visualization, Vis*, 2001. 5